Geomechanics and Engineering, *Vol. 19, No. 3 (2019) 255-268*
DOI: https://doi.org/10.12989/gae.2019.19.3.255

Support working resistance determined on top-coal caving face based on coal-rock combined body

Zhanbo Cheng[1,2,3], Shengli Yang*[1,2], Lianghui Li[1,2] and Lingfei Zhang[1,2]

[1]*School of Energy and Mining Engineering, China University of Mining and Technology-Beijing, Beijing 100083, China*
[2]*Coal Industry Engineering Research Center of Top-coal Caving Mining, Beijing 100083, China*
[3]*School of Engineering, University of Warwick, Coventry CV47AL, U.K.*

(Received June 29, 2019, Revised October 17, 2019, Accepted October 22, 2019)

Abstract. Taking top-coal caving mining face (TCCMF) as research object, this paper considers the combination of top-coal and immediate roof as cushion layer to build the solution model of support resistance based on the theory of elastic foundation beam. Meanwhile, the physical and mechanical properties of coal-rock combination influencing on strata behaviors is explored. The results illustrate that the subsidence of main roof in coal wall increases and the first weighting interval decreases with the increase of top-coal and immediate roof thicknesses as well as the decrease of top-coal and immediate roof elastic modulus. Moreover, the overlying strata reflecting on support has negative and positive relationship with top-coal thickness and immediate roof thickness, respectively. However, elastic modulus has limit influence on the dead weight of top-coal and immediate roof. As a result, it has similar roles on the increase of total support resistance and overlying strata reflecting on support in the limit range of roof control distance. In view of sensitive analysis causing the change of total support resistance, it can be regards as the rank of three components as immediate roof weight > overlying strata reflecting on support > top coal weight. Finally, combined with the monitoring data of support resistance in Qingdong 828, the validity of support resistance determined based on elastic foundation beam is demonstrated, and this method can be recommended to adopt for support type selecting in TCCMF.

Keywords: support resistance determination; elastic foundation beam; coal-rock combination; sensitive analysis

1. Introduction

China is the largest producer and consumer of coal in the World accounting to about half of the total coal production and consumption of the World, especially in recent years as shown in Fig. 1 (BP 2018). In the explored coal seam storage, the thick coal seam (thickness ≥3.5m) in China is rich in reserves and production accounting for about 45% of the total coal seam reserves and production (Wang *et al.* 2014, Zhang *et al.* 2019, Cheng *et al.* 2019). Thus, it is also the pillar industry of national economy and has a pivotal strategic position (Wang *et al.* 2015). At present, there are three methods of slice mining, large cutting height mining and top-coal caving mining adopted in thick coal seam mining (Alehossein and Poulsen 2010, Cheng *et al.* 2018, Kong *et al.* 2019, Liu and Cheng 2019, Liu *et al.* 2018, Lv *et al.* 2019, Suchowerska *et al.* 2015). Among of these methods, top-coal caving mining can achieve high efficiency and effective production of coal, reduce the quantities of roadway excavation and the number of workface moving, decrease material consumption under complex geological conditions and coal seam occurrence conditions (e.g. steep inclined thick coal seam). Therefore, the cost of coal per ton has significant reduction. Top-coal caving mining occupies a dominant position in thick coal seam mining due to the obvious technical and economic advantages (Basarir *et al.* 2015, Wang 2018, Wang *et al.* 2014, Alehossein and Korinets 2000, Hock and Brown 1997).

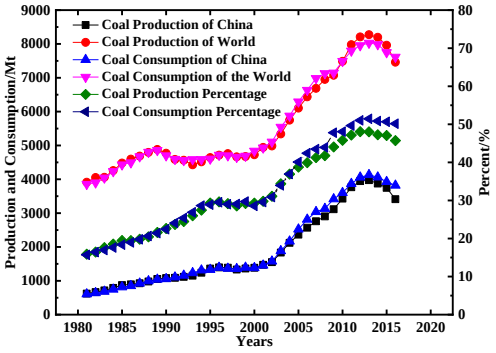

Fig. 1 Coal production and consumption of China and the world

As one of the most quantitative parameters to ensure the safety mining and machine selection in workface, support working resistance has been paid attention in recent decades. However, there are relatively few mines in foreign countries adopting top-coal caving mining because of the different of coal seam occurrence conditions. Therefore, the references about the support working resistance determined in TCCMF are limited to find. And thick coal seam using

*Corresponding author, Associate Professor
E-mail: yslcumtb@163.com

ISSN: 2005-307X (Print), 2092-6219 (Online)

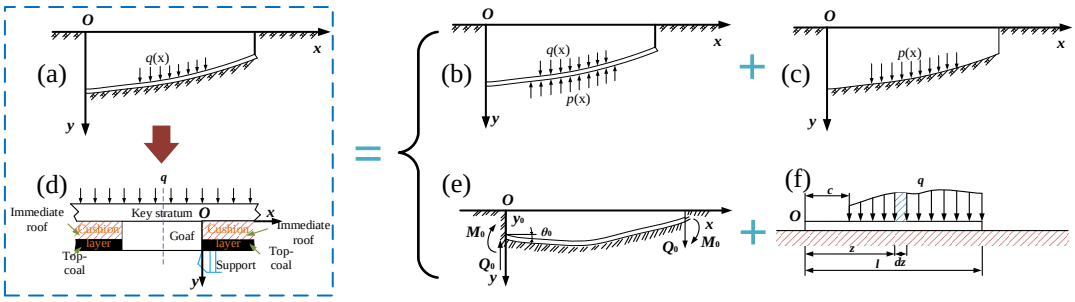

Fig. 2 Mechanical model of elastic foundation beam

top-coal caving mining technology or similar methods are mainly concentrated in Australia, India, Turkey, Russia and Slovenia (Alehossein and Poulsen 2010, Basarir *et al.* 2015, Kirzhner and Rozenbaum 2001, Masri *et al.* 2014, Vakili and Hebblewhite 2010, Yasitli and Unver 2005, Yang *et al.* 2018). In term of TCCMF, the determination method of support working resistance is enriched on the basis of drawing on the determination of the working resistance of the support in fully mechanized mining face, such as empirical equations, self-weight method, damage mechanics method, back-analysis numerical simulation method (Guo *et al.* 2018, Lei *et al.* 2016, Yasitli and Unver 2005, Xie and Zhao 2009, Xie *et al.* 2009, Alejano *et al.* 1999, Marschalko *et al.* 2011, Sasaoka *et al.* 2015). Although these method can be easily and conveniently adopted to estimate support working resistance, the larger error is also found causing the under-estimated or over-estimated for support working resistance. Therefore, there are potential security problems or excessive cost for equipment selection.

It should be noted that the occurrence of top-coal in TCCMF combined with immediate roof can be regards as cushion layer to transfer the overlying strata on support. However, there are limit references to describe the support working resistance determined considering the top-coal and immediate roof as a combined body. Therefore, the aims of this study is to build mechanical models of first and periodic weighting for obtaining analytical solutions of overlying strata reflecting on support in the limit range of roof control distance based on elastic foundation beam theory. Moreover, the influence of top-coal thickness, immediate roof thickness, top-coal elastic modulus and immediate roof elastic modulus on first weighting interval and support working resistance is analyzed. Taking Qingdong 828 as engineering background, the applicability of support working resistance determined method proposed in this study is verified and the new support resistance determined method provides the theoretical guideline for support type selection.

2. Basic equations of Winkler model

According to Winker model, load undertook in unit area is positive with the subsidence of surface as follows

$$\sigma = k_0 y \tag{1}$$

where σ is bearing pressure each unit area, y is the subsidence of foundation, k_0 is foundation coefficient, which can be approximately calculated by Eq. (2).

$$k_0 = \frac{E}{H} \tag{2}$$

where H and E are the thickness and elastic modulus of cushion, respectively. In terms of top coal-immediate roof combined body, H represents the total thickness of top-coal and immediate roof. Cheng *et al.* (2018) given the expression of elastic modulus as follows

$$E = \frac{k'}{A} = \frac{E_1 E_2 (r+1)^2}{E_1 + E_2 r^2 + 2r\sqrt{E_1 E_2}} \tag{3}$$

where k' is pull-pressing rigidity, E_1 and E_2 are the elastic modulus of coal mass and rock mass, respectively. r is coal to rock height ratio. Meanwhile, the relationship between foundation stress in the unit length of beam (p) and its pressure can be expressed as follows

$$p = \sigma b \tag{4}$$

where b is the width of beam. Another expression of Winker Model can be shown as Eq. (5).

$$p = ky \tag{5}$$

Obviously, k is the product of foundation coefficient and beam width. Fig. 2 is the schematic of mechanical model of elastic foundation beam. In this model, the bearing stress of beam and the interactive stress between beam and foundation can be presented with q(x) and p(x), respectively. Moreover, the stress analysis of foundation-beam can be divided into the stress analysis of beam and the stress analysis of foundation separately as shown in Fig. 2 (b) and (c), respectively.

In terms of Fig. 2 (b), the foundation settlement function y(x), foundation pressure p(x), overlying strata pressure q(x) should satisfy the following equation, which can be regards as basic differential equation of elastic foundation beam to obtain the result of foundation settlement.

$$EI\frac{d^4 y}{dx^4} + ky = q(x) \tag{6}$$

where EI is the flexural rigidity of beam section. Defined the characteristic coefficient (β) as follows

$$\beta = \sqrt[4]{\frac{k}{4EI}} \tag{7}$$

Substituting Eq. (7) to (6), it can be obtained another expression of basic differential equation as follows

$$\frac{d^4y}{dx^4}+4\beta^4y=\frac{q(x)}{EI} \tag{8}$$

Therefore, the general solution of Eq. (8) can be expressed as follows

$$\begin{aligned} y&=e^{\beta x}(A\cos\beta x+B\sin\beta x)\\ &+e^{-\beta x}(C\cos\beta x+D\sin\beta x)+y_1(x)\end{aligned} \tag{9}$$

The foundation settlement function can be acquired through four constant parameters of A, B, C, D which can be determined through four boundary conditions. Especially, in long beam model, the value of A and B can be regards as zero because there is a little influence on infinity location caused by loading, whereas the value of A and B is uncertain in short beam model owing to the effect of loading on the end of beam not disappearing. In this condition, the initial parameter method is usually adopted to solve the function of y(x) expressed by initial settlement (y_0), rotation angle (θ_0), bending moment (M_0) and shear force (Q_0).

3. Mechanical model of key stratum

3.1 Solution of key stratum deflection

Before initial weight occurring, the mechanical model of TCCMF is shown in Fig. 2(d) and the coordinate system of half beam is established. Taking the boundary of goaf as coordinate origin, the middle of goaf can be expressed as $-l$. Therefore, the settlement function of key stratum can be presented with the different horizontal location.

$$E_1I_1\frac{d^4y}{dx^4}=q_1 \quad (-l\le x\le 0) \tag{10}$$

$$E_1I_1\frac{d^4y}{dx^4}=q_1-k_1y_1 \quad (0\le x\le\infty) \tag{11}$$

where q_1 is the distributed load including its gravity of key stratum. The mechanical model of foundation-beam can be divided into non-loading mechanical model and only distributed loading mechanical model as shown in Fig. 2 (e). In non-loading mechanical model, the external force only effects on both ends of beam which means q(x) equaling to zero. Therefore, the defection equation y(x) can be obtained according to Eq. (9).

$$y=e^{\beta x}(A\cos\beta x+B\sin\beta x)+e^{-\beta x}(C\cos\beta x+D\sin\beta x) \tag{12}$$

At the same time, the rotation angle, bending moment and shearing force of key stratum can also achieved as Eqs. (13) ~ (15).

$$\theta=\frac{dy}{dx}=\beta\left\{e^{\beta x}\left[(A+B)\cos\beta x+(B-A)\sin\beta x\right]-e^{-\beta x}\left[(C-D)\cos\beta x+(C+D)\sin\beta x\right]\right\} \tag{13}$$

$$M=-EI\frac{d\theta}{dx}=-2EI\beta^2\left\{e^{\beta x}\left[B\cos\beta x-A\sin\beta x\right]-e^{-\beta x}\left[D\cos\beta x-C\sin\beta x\right]\right\} \tag{14}$$

$$Q=\frac{dM}{dx}=-2EI\beta^3\left\{e^{\beta x}\left[(B-A)\cos\beta x-(A+B)\sin\beta x\right]+e^{-\beta x}\left[(C+D)\cos\beta x-(C-D)\sin\beta x\right]\right\} \tag{15}$$

Substituting boundary conditions into Eqs. (13) ~ (15), the relationship between four integral constants and four initial parameters can be expressed as follows

$$\begin{aligned} A&=\frac{y_0}{2}+\frac{\theta_0}{4\beta}+\frac{Q_0}{8EI\beta^3}\\ B&=\frac{\theta_0}{4\beta}-\frac{M_0}{4EI\beta^2}-\frac{Q_0}{8EI\beta^3}\\ C&=\frac{y_0}{2}-\frac{\theta_0}{4\beta}-\frac{Q_0}{8EI\beta^3}\\ D&=\frac{\theta_0}{4\beta}+\frac{M_0}{4EI\beta^2}-\frac{Q_0}{8EI\beta^3}\end{aligned} \tag{16}$$

Defined Krylov Function as follows

$$\begin{aligned} \phi_1&=\mathrm{ch}\beta x\cos\beta x\\ \phi_2&=\mathrm{ch}\beta x\sin\beta x+\mathrm{sh}\beta x\cos\beta x\\ \phi_3&=\frac{1}{2}\mathrm{sh}\beta x\sin\beta x\\ \phi_4&=\frac{1}{4}(\mathrm{ch}\beta x\sin\beta x-\mathrm{sh}\beta x\cos\beta x)\end{aligned} \tag{17}$$

where $\mathrm{ch}\beta x=\frac{e^{\beta x}+e^{-\beta x}}{2}$, $\mathrm{sh}\beta x=\frac{e^{\beta x}-e^{-\beta x}}{2}$

Therefore, according to Eqs. (12) ~ (17), the analytic expressions of deflection, rotation angle, bending moment and shearing force of key stratum can be finally obtained on the situation of non-loading as follows

$$\begin{aligned} y&=y_0\cdot\phi_1+\frac{\theta_0}{\beta}\cdot\phi_2-M_0\cdot\frac{1}{EI\beta^2}\phi_3-Q_0\cdot\frac{1}{EI\beta^3}\phi_4\\ \theta&=-y_0\cdot4\beta\phi_4+\theta_0\cdot\phi_1-M_0\cdot\frac{1}{EI\beta}\phi_2-Q_0\cdot\frac{1}{EI\beta^2}\phi_3\\ M&=y_0\cdot4EI\beta^2\phi_3+\theta_0\cdot4EI\beta\phi_4+M_0\cdot\phi_1+\frac{Q_0}{\beta}\phi_2\\ Q&=y_0\cdot4EI\beta^3\phi_2+\theta_0\cdot4EI\beta^2\phi_3-M_0\cdot4\beta\phi_4+Q_0\cdot\phi_1\end{aligned} \tag{18}$$

On the other hand, if there is distributed loading effecting on foundation beam as shown in Fig. 2 (f), the correction term of deflection should be added in any section. To be specific, the loading of a small segment dz which is at the distance of z from origin point can be expressed as follows

$$\mathrm{d}p=q(z)\mathrm{d}z \tag{19}$$

Therefore, the correction value of deflection caused on the right of this segment is shown in Eq. (20).

$$q(z)dz\cdot\frac{1}{EI\beta^3}\phi_4\left[\beta(x-z)\right] \tag{20}$$

Based on the above equation, the total correction value at x point can be obtained through integral from origin point to x point.

$$\text{Total correction term}=\frac{1}{EI\beta^3}\int_0^x q(z)\phi_4\left[\beta(x-z)\right]dz \tag{21}$$

However, when the distributed loading is uniform, there is obviously no correction term on the range from origin point to c point (Fig. 2 (f)), whereas the correction term in the range from c point to l point is expressed as Eq. (22).

$$\text{Total correction term}=\frac{q}{EI\beta^3}\int_c^x\phi_4\left[\beta(x-z)\right]dz \tag{22}$$

According to $\phi_1(0)=1$ and the correspondingly ntegral, it

can be obtained as follows

$$\int_c^x \phi_4[\beta(x-z)]dz = \frac{1}{4\beta}\phi_1[\beta(x-z)]\Big|_{z=c}^{z=x} = \frac{1}{4\beta}\{1-\phi_1[\beta(x-c)]\} \quad (23)$$

Simplification as follows

$$\text{Total correction term}=\|_c \frac{q}{k}\{1-\phi_1[\beta(x-c)]\} \quad (24)$$

Due to c equaling to zero when the initial weighting occurs, the settlement function of foundation can be expressed as follows

$$y = y_0\cdot\phi_1 + \frac{\theta_0}{\beta}\cdot\phi_2 - M_0\cdot\frac{1}{EI\beta^2}\phi_3 - Q_0\cdot\frac{1}{EI\beta^3}\phi_4 + \frac{q}{k}[1-\phi_1(\beta x)] \quad (25)$$

Combined with boundary conditions and continuous conditions, the subsidence value of key stratum on initial weighting in different location as follows

$$y=\frac{q_1}{E_1I_1}[\frac{1}{24}x^4+\frac{1}{6}lx^3+\frac{1}{4}l^2(1-2\alpha)x^2+\frac{1}{6}l^3(1-6\alpha)x+(\frac{1}{\beta l}+\frac{1}{2}-\alpha)\frac{l^2}{2\beta^2}] \quad (-l\le x\le 0) \quad (26)$$

$$y=\frac{q_1l^2}{2E_1I_1\beta^2}e^{-\beta x}[(\frac{1}{\beta l}+\frac{1}{2}-\alpha)\cos\beta x+(\alpha-\frac{1}{2})\sin\beta x] \quad (0\le x\le\infty) \quad (27)$$

where $\alpha=\dfrac{\beta^2l^2+3\beta l+3}{3\beta l(2+2\beta l)}$

Obviously, when β is towards to infinity as a result of k trending to infinity, α is equal to 1/6.

3.2 First caving distance of key stratum

The bending moment in the middle of key stratum (M_α) can be expressed as follows

$$M_\alpha = EIy''_{-l} = \alpha q_1 l^2 \quad (28)$$

Obviously, the maximum bending moment (M_β) of key stratum can be obtained when the third-order derivative of deflection equals to zero as follows

$$M_\beta = -q_1l^2e^{-\beta x_\beta}\left[(\frac{1}{\beta l}+\frac{1}{2}-\alpha)\sin\beta x_\beta+(\frac{1}{2}-\alpha)\cos\beta x_\beta\right] = -Yq_1l^2 \quad (29)$$

where $Y=e^{-\beta x_\beta}\left[(\dfrac{1}{\beta l}+\dfrac{1}{2}-\alpha)\sin\beta x_\beta+(\dfrac{1}{2}-\alpha)\cos\beta x_\beta\right]$

And the corresponding location in x-axis is calculated as Eq. (30). The initial broken of key stratum occurs on the location obtaining maximum moment bending. According to Eqs. (28) and (29), if the value of α is larger than Y, the maximum bending moment can be expressed as follows

$$x_\beta = \frac{1}{\beta}\arctan\frac{1}{1+\beta l-2\alpha\beta l} \quad (30)$$

$$M_{\max} = \alpha q_1 l^2 \quad (31)$$

According to the strength theory of beam, the maximum stress can be achieved as follows

$$\sigma_{\max} = \frac{M_{\max}}{W_c} = \frac{6\alpha q_1 l^2}{h_1^2} = \frac{1}{10}\sigma_c \quad (32)$$

The value of l can be solved combined with Eq. (32) and the expression of α, and the initial collapse of key stratum can be computed as Eq. (33).

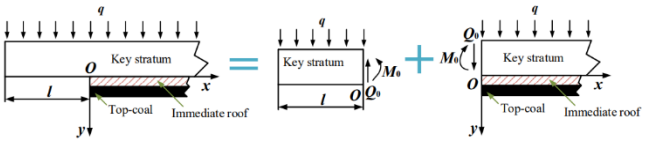

Fig. 3 Mechanical model periodic roof pressure

$$L_c = 2l + 2x_\beta \quad (33)$$

On the other hand, if Y is larger than α, the expression of l can also be described as follows

$$15q_1l^2e^{-\beta x_\beta}\left[(\frac{1}{\beta l}+\frac{1}{2}-\alpha)\sin\beta x_\beta+(\alpha-\frac{1}{2})\cos\beta x_\beta\right]-h_1^2\sigma_c=0 \quad (34)$$

The maximum broken interval of key stratum can be obtained as follow Eq. (35) when k trends to infinity.

$$L_c = h_1\sqrt{\frac{\sigma_c}{5q_1}} \quad (35)$$

3.3 Determination of support working resistance

3.3.1 Initial weighting stage

In terms of TCCMF, the total load caused by overlying strata effecting on any point from the rear of support can be presented as follows

$$P_1=\int_0^x yk_1dx=\int_0^x\frac{q_1l^2k_1}{2E_1I_1\beta^2}e^{-\beta x}\left[(\frac{1}{\beta l}+\frac{1}{2}-\alpha)\cos\beta x+(\alpha-\frac{1}{2})\sin\beta x\right]dx \quad (36)$$

Therefore, the support is subjected to the total overlying strata load in the range of roof-control distance as follows

$$P_1=D\left[(\frac{1}{\beta}+\beta l(1-2\alpha))e^{-\beta d}\sin\beta d-\frac{1}{\beta}e^{-\beta d}\cos\beta d+1\right] \quad (37)$$

where $D=\dfrac{q_1lk_1}{4E_1I_1\beta^4}$ and d is roof-control distance.

Considering the dead weight of top-coal and immediate roof, the total load effecting on support in the range of roof-control distance can be expressed as follows

$$P = P_1+P_2+P_3 = P_1+m_D\gamma_DL_EL+m_Z\gamma_ZL_EL \quad (38)$$

where P_2 is the dead weight of top-coal, P_3 is the dead weight of immediate roof, m_D is top-coal thickness, γ_D is the body force of top-coal, L_E is roof-control distance, L is the width of support, m_z is immediate roof thickness, γ_Z is the body force of immediate roof.

Therefore, combined with the actual engineering geological conditions of LTCC face, the trend of support load before initial weight can be achieved through Eq. (38) and the maximum support load is condition of initial collapse stage.

3.3.2 Periodic weighting stage

The mechanical model of periodic weighting on TCCMF is shown in Fig. 3 according to the characteristics of overlying strata, which can be divided into non-foundation stage and foundation stage.

The correction term of deflection can be expressed as

$$\frac{q}{k}\left[1-\phi_1(\beta x)\right]$$

Therefore, the analytic expression of defection, rotation angle, bending moment and shearing force of foundation beam in periodic weighting stage is shown in Eq. (39).

$$\begin{aligned} y &= y_0\cdot\phi_1+\frac{\theta_0}{\beta}\cdot\phi_2-M_0\cdot\frac{1}{EI\beta^2}\phi_3 \\ &\quad -Q_0\cdot\frac{1}{EI\beta^3}\phi_4+\frac{q}{k}\left[1-\phi_1(\beta x)\right] \\ \theta &= -y_0\cdot 4\beta\phi_4+\theta_0\cdot\phi_1-M_0\cdot\frac{1}{EI\beta}\phi_2 \\ &\quad -Q_0\cdot\frac{1}{EI\beta^2}\phi_3+\frac{4q\beta}{k}\phi_4 \\ M &= y_0\cdot 4EI\beta^2\phi_3+\theta_0\cdot 4EI\beta\phi_4 \\ &\quad +M_0\cdot\phi_1+\frac{Q_0}{\beta}\phi_2-\frac{4q\beta^2EI}{k}\phi_3 \\ Q &= y_0\cdot 4EI\beta^3\phi_2+\theta_0\cdot 4EI\beta^2\phi_3 \\ &\quad -M_0\cdot 4\beta\phi_4+Q_0\cdot\phi_1-\frac{4q\beta^3EI}{k}\phi_2 \end{aligned} \tag{39}$$

Combined with boundary conditions, the initial bending moment and shearing force are presented as follows

$$M_0=-\frac{1}{2}ql^2 \tag{40}$$

$$Q_0=-ql \tag{41}$$

Substituting Eqs. (40) and (41) into Eq. (39), the analytic expression of initial parameters can be shown as follows

$$y_0=\frac{q}{k}+\frac{ql^2}{4EI\beta^2}+\frac{ql}{2EI\beta^3} \tag{42}$$

$$\theta_0=-\frac{ql^2}{2EI\beta}-\frac{ql}{2EI\beta^2} \tag{43}$$

The support load caused by overlying strata in periodic weighting stage can also be achieved as follows

$$P_1=\int_0^d pdx=\int_0^d kydx \tag{44}$$

Simplification

$$\begin{aligned} P_1 &= ql\left[2\phi_2(\beta d)-2\phi_3(\beta d)-\phi_1(\beta d)+1\right] \\ &\quad -ql^2\beta\left[\phi_2(\beta d)+2\phi_4(\beta d)-2\phi_3(\beta d)\right]+qd \end{aligned} \tag{45}$$

At the same time, it is necessary to consider the dead weight of top-coal and immediate roof in calculating the total support load during periodic weighting. It should be noted that the coal seam inclination has significant influence on total support load (TSL) through changing the component of overburden load. And the inclined even extremely inclined coal seam will be explored in the further research.

4. Engineering background

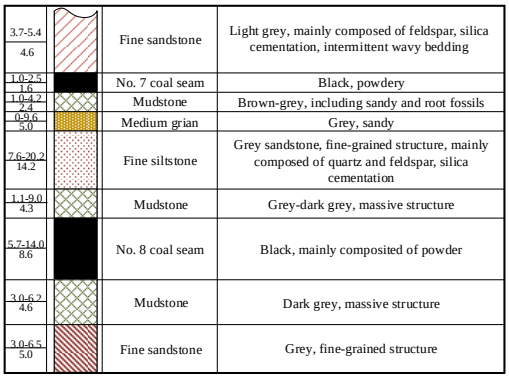

Fig. 4 Comprehensive stratigraphic column of 828 working face

Table 1 Basic mechanical parameters of coal and rock mass in 828 working face

Layer name	Thickness (m)	Bulk density (kN/m^3)	Bulk modulus (GPa)	Shear modulus (GPa)	Internal friction angle (°)	Cohesion (MPa)	Tensile strength (MPa)
Fine sandstone	4.6	25.9	3.65	2.62	35	2.8	1.7
#7 coal seam	1.6	14	2.67	1.60	25	1.5	0.8
Mudstone	2.4	26.4	3.15	2.07	27	2.0	1.0
Medium grain	5.0	24.2	3.42	2.21	30	2.2	1.4
Fine siltstone	14.2	30	6.5	4.88	39	8	4.5
Mudstone	4.3	26.4	3.15	2.07	27	2.0	1.0
#8 coal seam	8.6	13	2.43	1.39	25	1.5	0.8
Mudstone	4.6	26.4	3.15	2.07	27	2.0	1.0
Siltstone	5.0	26	4.14	2.98	35	3.2	2.0
Mudstone	5.0	26.4	3.15	2.07	27	2.0	1.0
Medium grain	10	24.2	3.42	2.21	30	2.2	1.4
Fine sandstone	15	25.9	3.65	2.62	35	2.8	1.7

5. Impact factors of support working resistance

Taking Qingdong 828 working face as engineering background, Fig. 5 illustrates the changes of roof subsidence, overlying strata applied on support, total support load along the advanced direction of working face in the limit range of roof-control distance based on the mentioned theoretical solution equations. As can be seen from Fig 5, roof subsidence reduces gradually from goaf to working face, while overlying strata load and total support load increase at the same condition along with the increment value decreasing. It indicates that the influence of roof-control distance on total support load (TSL) is greater than that of overlying strata load (OSL) under considering the self-weight of top-coal and immediate roof. Therefore, it is necessary to consider the influence of physical and mechanical parameters (top-coal thickness (TCT), immediate roof thickness (IRT), top-coal elastic modulus (TCEM), immediate roof elastic modulus (IREM)) of coal-rock combined body on roof subsidence, first caving

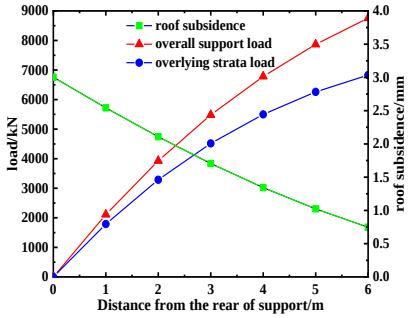

Fig. 5 Change laws of roof subsidence, loads in Qingdong 828 working face

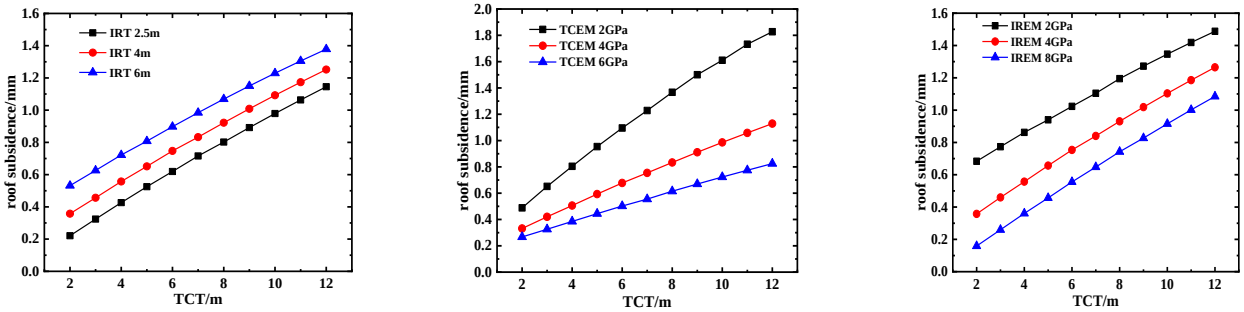

(a) various IRT (b) various TCEM (c) various IREM

Fig. 6 Roof subsidence versus TCT

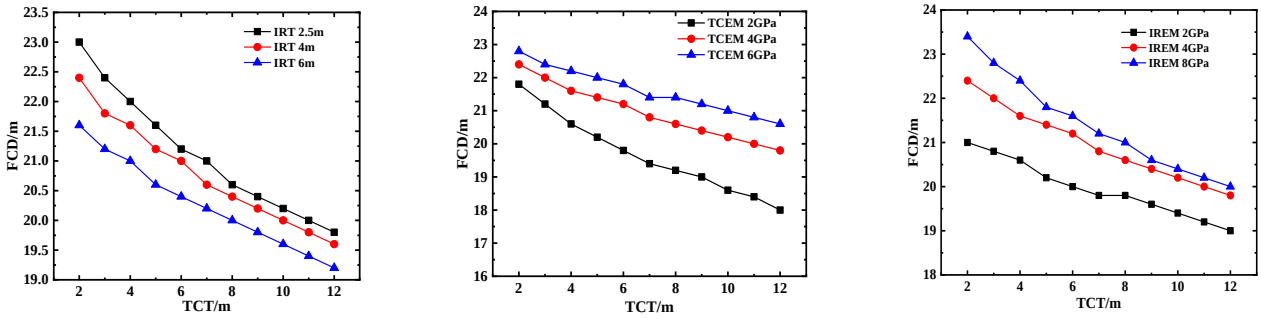

(a) various IRT (b) various TCEM (c) various IREM

Fig. 7 FCD versus TCT

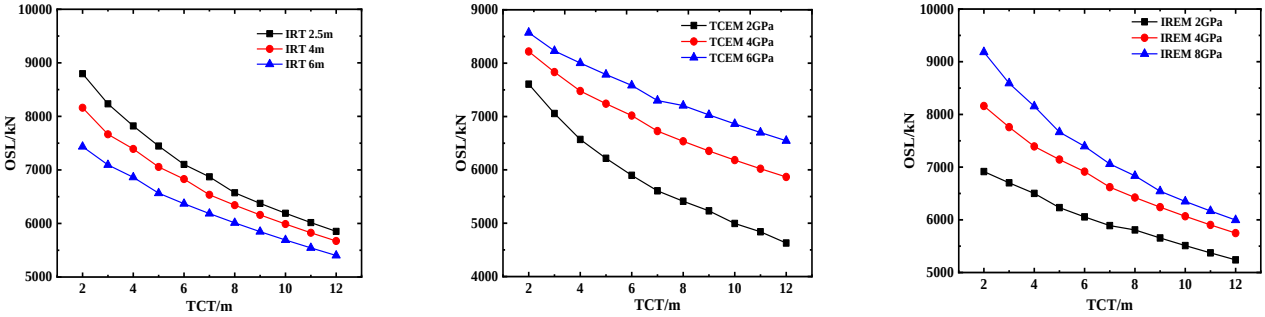

(a) various IRT (b) various TCEM (c) various IREM

Fig. 8 OSL versus TCT

distance (FCD), OSL and TSL. The details as follow.

5.1.1 Roof subsidence

Fig. 6 demonstrates the change of roof subsidence at the location of coal wall with an increase of TCT. There is approximately linear relationship between roof subsidence and TCT. However, the increment of roof subsidence exhibits great differences under various conditions. To be specific, the parameters of immediate roof have no obvious influence on the increment of roof subsidence with the increase of TCT, while the significant increment of roof subsidence can be observed under a small value of TCEM.

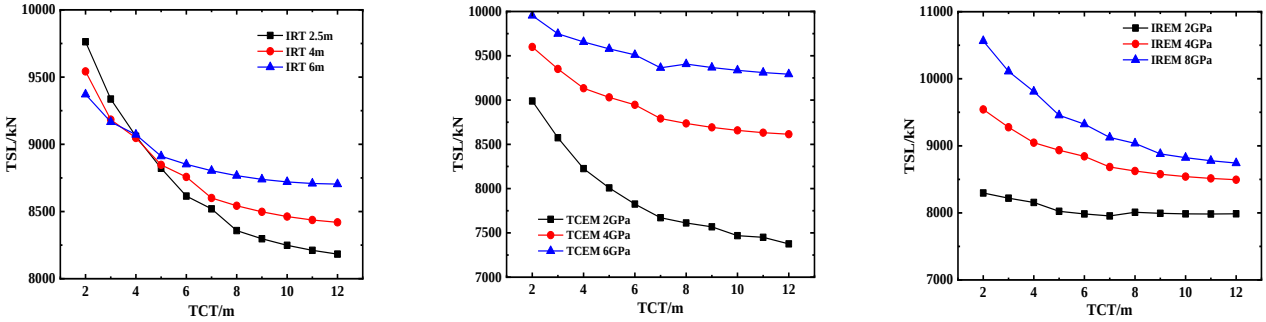

(a) various IRT (b) various TCEM (c) various IREM

Fig. 9 TSL versus TCT

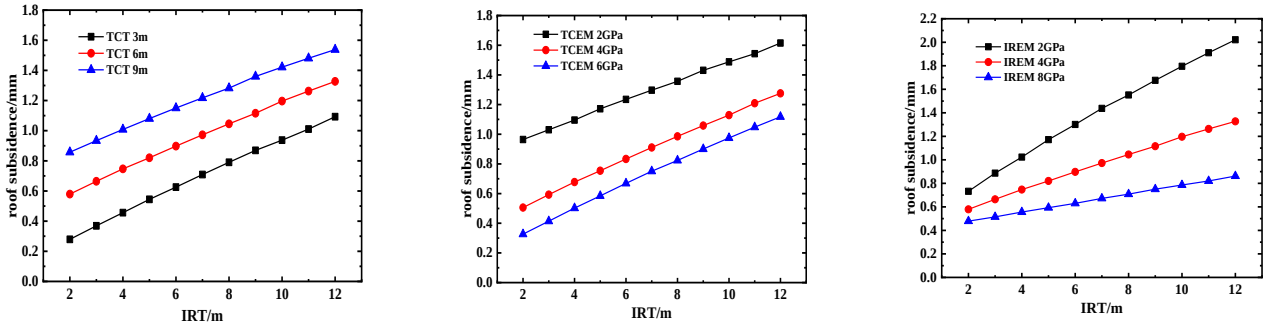

(a) various IRT (b) various TCEM (c) various IREM

Fig. 10 Roof subsidence versus IRT

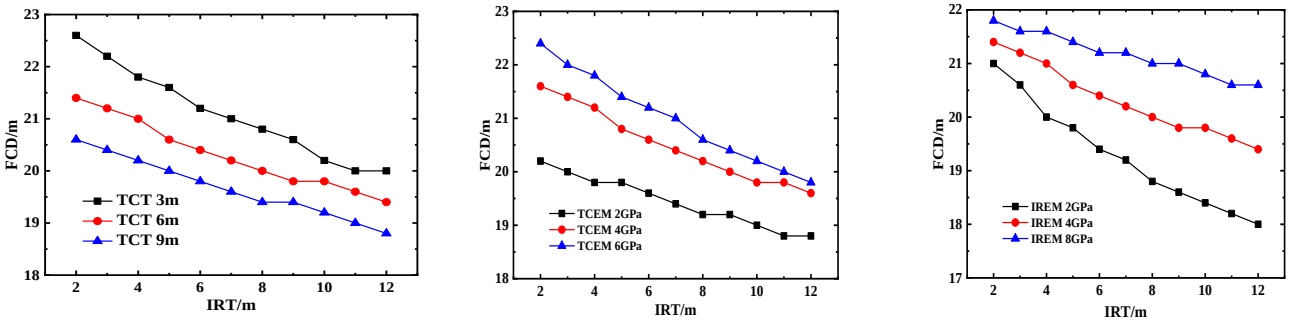

(a) various TCT (b) various TCEM (c) various IREM

Fig. 11 FCD versus IRT

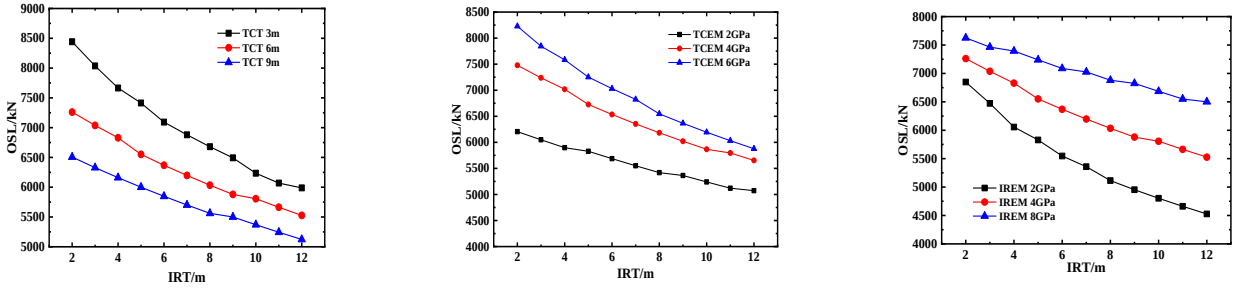

(a) various TCT (b) various TCEM (c) various IREM

Fig. 12 OSL versus IRT

5.1.1 Roof subsidence

Fig. 6 demonstrates the change of roof subsidence at the location of coal wall with an increase of TCT. There is approximately linear relationship between roof subsidence and TCT. However, the increment of roof subsidence exhibits great differences under various conditions. To be specific, the parameters of immediate roof have no obvious influence on the increment of roof subsidence with the increase of TCT, while the significant increment of roof subsidence can be observed under a small value of TCEM.

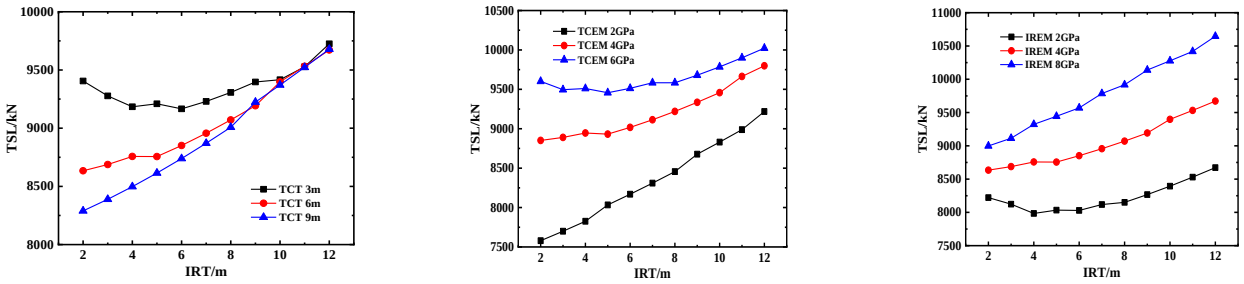

(a) various TCT (b) various TCEM (c) various IREM

Fig. 13 TSL versus IRT

5.1.2 First caving distance

Fig. 7 shows the relationship between FCD and TCT. Obviously, the increase of mining space causes by the increase of TCT. Therefore, there only requires small span of key strata to reach initial weighting. FCD almost linear decreases with the increase of TCT. However, the small TCEM leads to a greater decrement of FCD with the increase of TCT, while the opposite result can be found in terms of IREM. It should be noted that there is no obvious influence of IRT on the decrement of FCD. Therefore, in terms of the decrement of FCD with the increase of TCT, the mechanical properties of top coal and immediate roof have dominate location compared to IRT.

5.1.3 Overlying strata load applied on support in the range of roof-control distance

Fig. 8 illustrates the influence of TCT on overlying strata load (OSL) applied on support in the range of roof-control distance. Overall, the higher top-coal thickness means the smaller mining-caving ratio resulting in the small value of OSL acting on support in the limit range of roof-control distance. To be specific, OSL reduces and this trend gradual slowly with the increase of TCT. Similarly, IRT has limit influence on the decrement of OSL. On the other hand, a great decrement of OSL with the increase of TCT can be observed under the smaller TCEM and IREM.

5.1.4 Total support loading

Considering the self-weighing of top-coal and immediate roof in the range of roof-control distance, TSL versus TCT is shown in Fig. 9. Totally, the change laws of TSL are similar to OSL with the increase of TCT. It should be noted that although the self-weighting of top-coal increases with the increase of TCT, and this increment is smaller than the decrement of TSL influencing by OSL. Moreover, the decrement of TSL can be significantly observed with the increase of TCT under the smaller IRT. On the other hand, the small TCEM leading to the decrease of top-coal strength brings out a great decrement of TSL with the increase of TCT, which is opposite to IREM.

5.2 Immediate roof thickness

Similarly, in terms of explore the influence of IRT on the laws of strata behaviors in TCCMF, selecting any two of three parameters (TCT, TCEM, and IREM) remains constant and another one parameter increases. And the results of various parameters (roof subsidence, FCD, OSL, TSL) in the occurrence of first weighting with the increase of IRT are illustrated as follow.

5.2.1 Roof subsidence

Taking the location of coal wall as example, the roof subsidence in this point is illustrated with the increase of IRT as shown in Fig. 10. It can be found that roof subsidence linear increases with the increase of IRT. And the properties of top-coal have neglected influence on the increment of roof subsidence with the increase of IRT. Moreover, the IREM smaller, the increment value larger. Therefore, the behaviors of IREM plays dominant roles on the influence of IRT on roof subsidence than the characteristics of top-coal.

5.2.2 First caving distance

As shown in Fig. 11, FCD is illustrated almost linear decreasing with the increase of IRT. There is no significant decrement observed under considering the properties of top-coal. For example, FCD only reduces 2 m with IRT increasing from 2 m to 12 m under TCT 3 m. On the other hand, the smaller IREM can lead to a great decrement of FCD with the increase of IRT. On the basis of keeping mining height constant, the mining space and the exposure length of key strata absolutely increases with the increase of IRT causing main roof reaching initial collapse easily.

5.2.3 Overlying strata load applied on support in the range of roof-control distance

As shown in Fig. 12, although the increase of IRT has limit effective on roof subsidence and FCD, it contributes to a great influence on OSL. Generally, OSL decreases with the increase of IRT along with a small decrement firstly followed by tending to a certain value. The decrements of OSL are 2000kN, 1750kN and 1500kN with the increase of IRT from 2 m to 12 m under TCT 3 m, 6 m and 9 m, respectively. Therefore, the increase of IMT leads to a significant influence on the decrement of OSL under small TCT, large TCEM and small IREM.

5.2.4 Total support loading

As shown in Fig. 13, the trend of TSL increases with the increase of IRT because the self-weighting increment of immediate roof caused by the increase of IRT is greater than the decrement of OSL. To be specific, the increase of IMR has neglected influence on TSL under small TCT (e.g., 3 m). However, TSL increases continuously with the increase

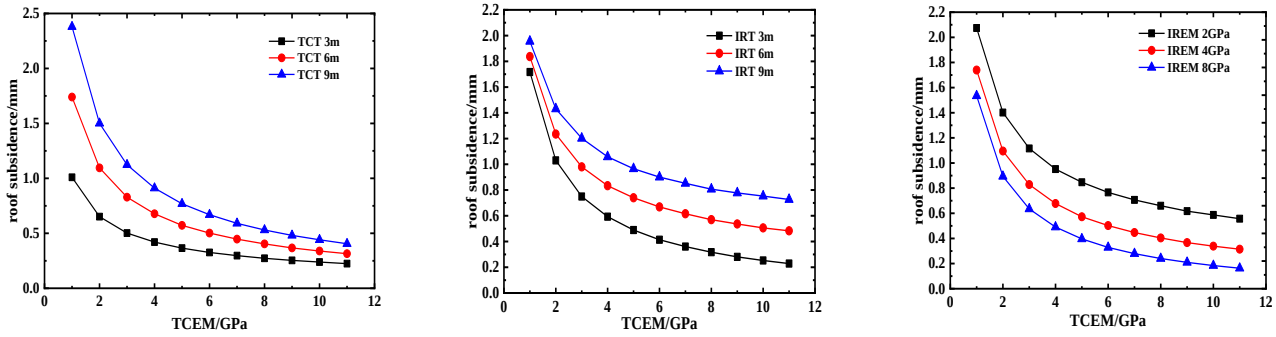

(a) various TCT (b) various IRT (c) various IREM

Fig. 14 Roof subsidence versus TCEM

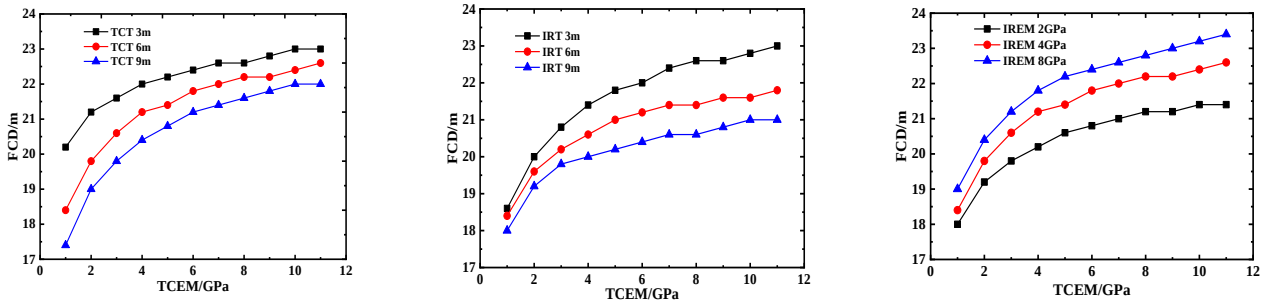

(a) various TCT (b) various IRT (c) various IREM

Fig. 15 FCD versus TCEM

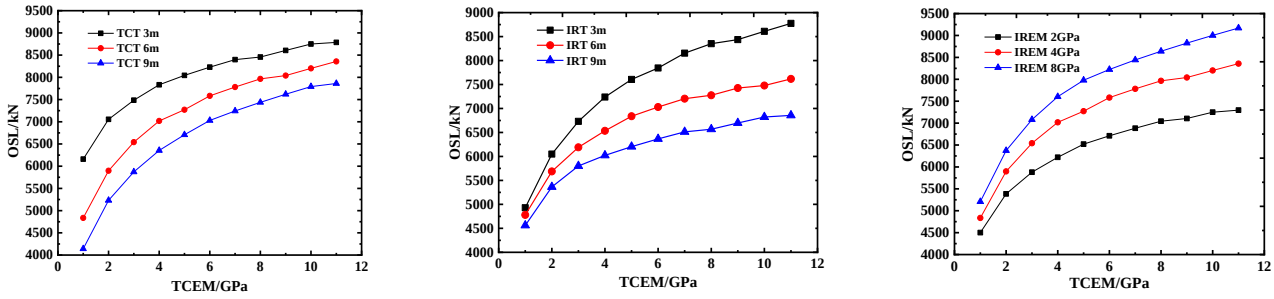

(a) various TCT (b) various IRT (c) various IREM

Fig. 16 OSL versus TCEM

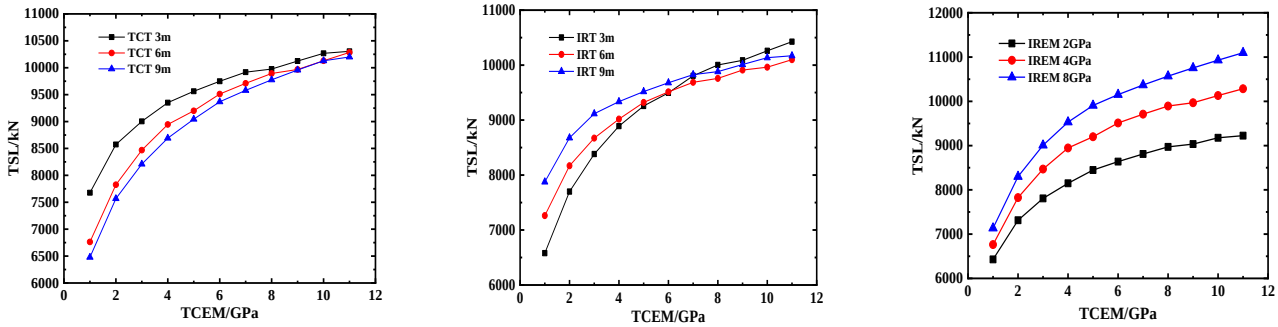

(a) various TCT (b) various IRT (c) various IREM

Fig. 17 TCL versus TCEM

of IMR with TCT reaching to a certain value. And when TCT is enough large, the increase of IMR cannot influence the change of TSL. On the other hand, the small TCEM and large IREM make a significant increment of TSL. It should be noted that TSL decreases followed by increasing with the increase of IRT under a small IREM. Generally, the influence of OSL on TSL tends to slow considering the self-weighting of top-coal and immediate roof. And the change of IRT influencing on TSL is greater than OSL and then TCT.

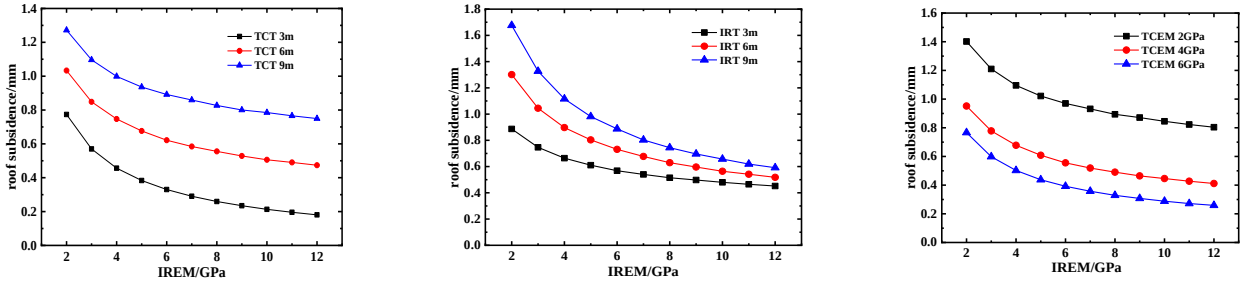

(a) various TCT (b) various IRT (c) various TCEM

Fig. 18 Roof subsidence versus IREM

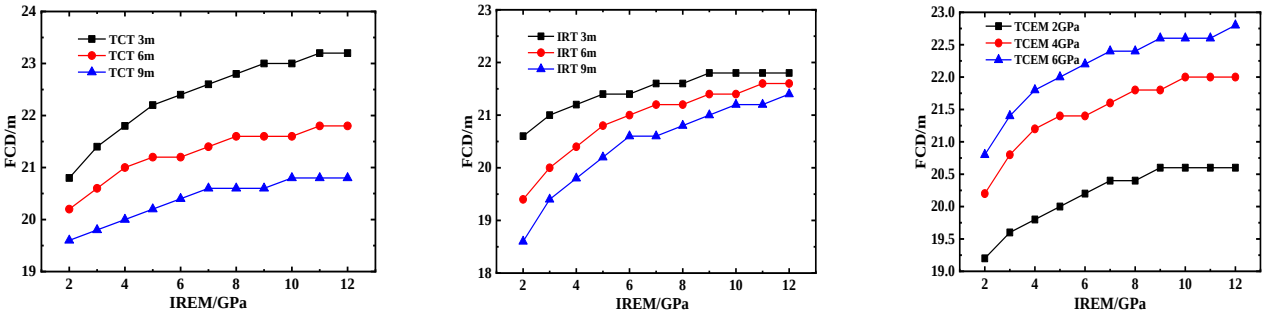

(a) various TCT (b) various IRT (c) various TCEM

Fig. 19 FCD versus IREM

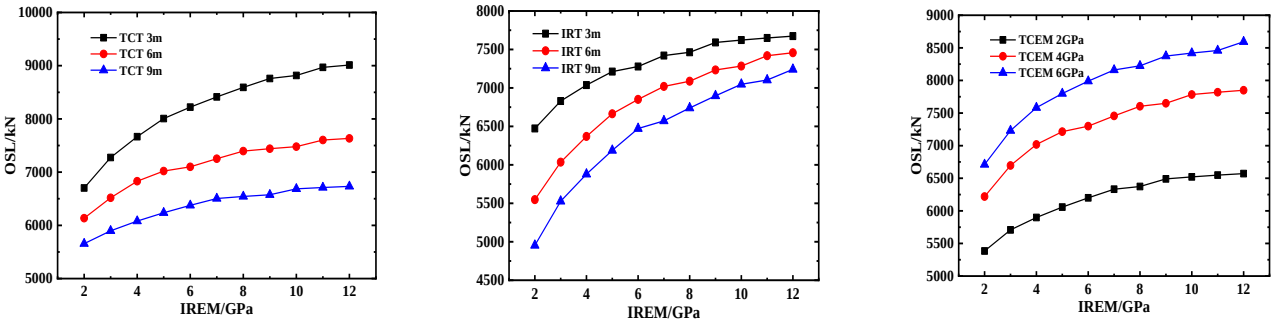

(a) various TCT (b) various IRT (c) various TCEM

Fig. 20 OSL versus IREM

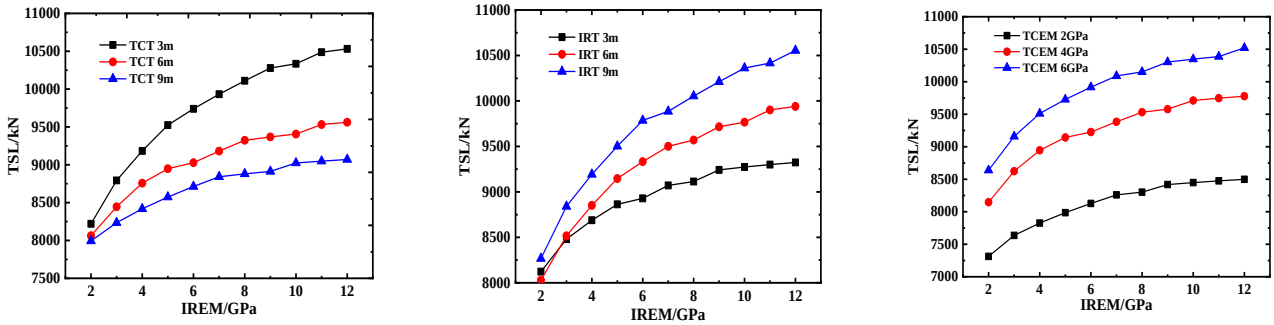

(a) various TCT (b) various IRT (c) various TCEM

Fig. 21 TSL versus IREM

5.3 Elastic modulus of top-coal

TCEM can reflect the strength and integrity of top-coal. In order to analyze the influence of TCEM on the relative parameters of strata behaviors in TCCMF, two of three parameters (TCT, IRT and IREM) remain constant. The details are discussed as follow.

5.3.1 Roof subsidence

Selecting the point of coal wall to monitor roof subsidence, its tendency with the increase of TCEM can be revealed in Fig. 14. In general, the bearing ability of top-

coal possessing large elastic modulus is high due to the better integrity. Therefore, roof subsidence decreases gradually with the increase of TCEM along with the slope of curve tending to slow. It means roof subsidence cannot be observed significant change if TCEM reaches to a certain value. Especially for high TCT and small IRT, TCEM is of great importance to determine the roof subsidence of key strata in coal wall.

5.3.2 First caving distance

The change laws of FCD with the increase of TCEM are shown in Fig. 15. Generally, FCD increases with the increase of TCEM due to the excellent bearing ability. And when TCEM reaches to a certain value, FCD towards fixed value as well. It should be noted that the increase of TCEM contributes to a great increment of FCD under large TCT and IREM, small IRT.

5.3.3 Overlying strata load applied on support in the range of roof-control distance

As can be seen in Fig. 16, OSL increases with the increase of TCEM and its increment tends to stable. To be specific, the increments of OSL are 2500kN, 3000kN, 3500kN with TCEM increasing from 1GPa to 11GPa under TCT 3 m, 6 m and 9 m, respectively. That means large TCT causing a significant increment of OSL along with the same increment of TCEM. Similarly, this results can also be revealed in small IRT and large IREM.

5.3.4 Total support loading

Fig. 17 illustrates the relationship of TSL versus TCEM. Similarly with OSL, TSL increases with the increase of TCEM as well. A large TCT or IREM, and small IRT lead to a significant increment of TSL with the increase of TCEM. However, TCT and IRT cannon contribute the value of TSL if TCEM reaches to a certain value (e.g. 7GPa). And if TCEM is less than 1GPa, IREM also does not influence the value of TSL as shown in Fig. 17 (c).

5.4 Elastic modulus of immediate roof

Similarly, the strength and integrity of immediate roof are determined by its elastic modulus. And any two of three parameters (TCT, IRT and IREM) keep constant to analyze the influence of IREM on strata behaviors as follow.

5.4.1 Roof subsidence

Roof subsidence in the position of coal wall is explored with the increase of IREM. Obviously, roof subsidence decreases with the increase of IREM and reaches to a certain value under IREM larger than 10GPa. Due to the curves of roof subsidence versus IREM paralleling with various TCTs and TCEMs, the properties of top-coal have no roles on the influence of IREM on the decrement of roof subsidence. On the other hand, large IRT causes a great influence of roof subsidence decrement with the increase of IREM.

5.4.2 First caving distance

As shown in Fig. 19, FCD increases with the increase of IREM and its increment tends to stable. Moreover, small TCT and large IRT lead to a significant increment of FCD with a same increment of IREM, while there is no obvious change observed under different TCEM conditions.

5.4.3 Overlying strata load applied on support in the range of roof-control distance

The relationship of OSL versus IREM is shown in Fig. 20. The data shows that OSL increases with the increase of IREM. Moreover, small TCT, large IRT and TCEM make OSL greatly change under different IREM.

5.4.4 Total support loading

Considering the self-weighting of top-coal and immediate roof, the change of TSL with the increase of IREM can be demonstrated as Fig. 21. Obviously, the increase of IREM can contribute to the increase of TSL. And the increment of TSL is significantly observed under small TCT and large IRT conditions. However, the value of TCEM has limit influence on the increment of TCL with the increase of IREM.

6. Case study

6.1 Monitor point layout

From the begin to end of working face, measuring pressure devices are installed in various supports (S1#, S2#, S10#, S20#, S30#, S40#, S50#, S60#, S70#, S80#, S85# and S86#) with a same interval. The layout details as shown in Fig. 22. For analyzing strata behaviors accuracy, all supports can be divided into three parts with upper (S1#, S2#, S10#, S20#), middle (S30#, S40#, S50#, S60#) and lower (S70#, S80#, S85#, S86#) zones.

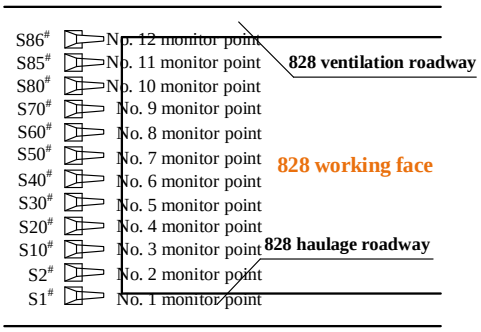

Fig. 22 Monitor point layout in Qingdong 828 working face

Table 2 Weight step of 828 working face

Type		Lower	Middle	Upper	Average
FCD (m)		22.0	20.1	20.7	20.9
Periodic caving distance (m)	First periodic	10.0	12.7	10.5	11.1
	Second periodic	9.8	12.2	13.8	11.9
	Third periodic	11.8	10.2	9.6	10.5
	Forth periodic	9.2	10.5	8.8	9.5
	Fifth periodic	11.0	11.0	12.5	11.5
	Average	10.36	11.32	11.04	10.91

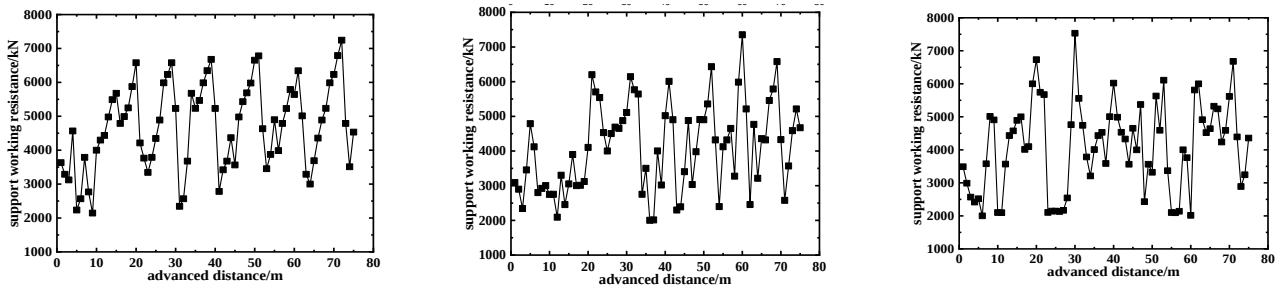

(a) upper (b) middle (c) lower

Fig. 23 Monitor results

Table 3 Physical and mechanical parameters of coal

Parameter	Coal body	Rock body	Coal-rock combined body
Elastic modulus/GPa	3.5	5.09	4.05
Bulk modulus/GPa	2.43	3.15	-
Shear modulus/GPa	1.39	2.07	-
Thickness/m	6.1	4.3	10.4
Self-weighting/kN	750.75	1191.96	1942.71

6.2 Monitor results

Taking S2#, S40# and S80# as example, the monitoring results are shown in Fig. 23 and Table 2. FCD, periodic caving distance and support working resistance can be illustrated as follow. FCD in lower, middle and upper of working face is 22 m, 20.1 m and 20.7 m, respectively. Therefore, FCD in Qingdong 828 working face can be regards as 21 m. In terms of periodic caving distance, the average value is 11m. Moreover, the maximum support working resistance in all processes is approximately 8000kN.

6.3 Theory results

According to the theory of elastic-plastic mechanics, the relationship of elastic modulus (E), bulk modulus (K) and shear modulus (G) can be expressed as follows

$$E = \frac{9KG}{3K + G} \tag{46}$$

Based on the current geology information and taking roof-control distance as 6 m, the coal and rock samples were collected in-site and then carried out physical and mechanics experiments to obtain the relative parameters as shown in Table 3.

Moreover, the first caving of key strata is occurred on the middle location of goaf and FCD can be calculated as 22.4m, which is match with the monitor result in practice. Combined with the overlying load of 420kPa, OSL applied on support in roof-control distance is 5313.3kN. Therefore, TSL under first caving of key strata is 7447.9kN.

In the period of periodic caving, the overlying load decreases to 183kPa and periodic caving distance is 11m as mentioned before. Therefore, TSL in roof-control distance is 6242kN. Selecting safety factor as 1.1, the theory values of TSL are 8192.69kN and 6866kN in initial weighting and periodic weighting, respectively, which are match with the monitor results. Therefore, the required support working resistance in design is 8400kN to provide the guideline of support type selection.

7. Conclusions

Taking coal-rock combined body as foundation and based on the theory of elastic foundation to establish the mechanical modulus of initial weight and periodic weighting, the deflection of key strata can be obtained. Moreover, overlying strata load applied on support in the range of roof-control distance and total support load considering the self-weight of top-coal and immediate roof are illustrated to provide guideline for the selection of support type. The details of conclusions as follow.

1) The roof subsidence of key strata gradually reduces along the advancing direction of working face within the range of roof-control distance. Taking the position of coal wall as example, roof subsidence almost linear increases with the increase of TCT and IRT. And the significant increment of roof subsidence can be observed under small TCEM and IREM. On the other hand, roof subsidence gradually decreases with the increase of TCEM and IREM.

2) With the increase of TCT and IRT, FCD exhibits almost linear decreasing, while FCD increases with the increase of TCEM and IREM along with its tendency reducing. In general, the physical and mechanical parameters of top-coal and immediate roof have limit influence on FCD.

3) OSL and TSL decrease with the increase of TCT due to a higher TCT performing good cushion effective, while TSL increases with the increase of IRT because the self-weighting rising is greater than that of cushion effective leading to the decrease of OSL. Moreover, OSL and TSL increase with the increase of TCEM and IREM along with its slope tending to stable. Through sensitive analysis for three parts influencing on TSL, the ranking can be expressed as immediate roof weight > overlying strata reflecting on support > top coal weight.

4) Taking Qingdong 828 working face as engineering background, the results of theory calculation is high match with monitoring data in practice. It indicates the method of determined support working resistance based on the mechanical properties of coal-rock combined body is reasonable and accuracy.

Acknowledgments

The authors wish to acknowledge the support from China Scholarship Council (CSC), the National Natural Science Foundation of China (No. 51974320) and the National Key Research and Development Project (No. 51934008). The authors would also like to thank the editors and anonymous reviewers for their valuable time and suggestions.

References

Alehossein, H. and Korinets, A. (2000), "Mesh-independent finite difference analysis using gradient-dependent plasticity", *Commun. Numer. Meth. Eng.*, **16**(5), 363-375. https://doi.org/10.1002/(SICI)1099-0887(200005)16:5%3C363::AID-CNM344%3E3.0.CO;2-W.

Alehossein, H. and Poulsen, B.A. (2010), "Stress analysis of longwall top coal caving", *Int. J. Rock Mech. Min. Sci.*, **47**(1), 30-41. https://doi.org/10.1016/j.ijrmms.2009.07.004.

Alejano, L.R., Ramirez-Oyanguren, P. and Taboada, J. (1999), "FDM predictive methodology for subsidence due to flat and inclined coal seam mining", *Int. J. Rock Mech. Min. Sci.*, **36**(4), 475-491. https://doi.org/10.1016/S0148-9062(99)00022-4.

Basarir, H., Oge, I.F. and Aydin, O. (2015), "Prediction of the stresses around main and tail gates during top coal caving by 3D numerical analysis", *Int. J. Rock Mech. Min. Sci.*, **76**, 88-97. https://doi.org/10.1016/j.ijrmms.2015.03.001.

BP (2018), "BP Statistical review of world energy", British Petroleum, London, U.K.

Cheng, Z.B., Li, L.H. and Zhang, Y.N. (2019), "Laboratory investigation of the mechanical properties of coal-rock combined body", *Bull. Eng. Geol. Environ.* https://doi.org/10.1007/s10064-019-01613-z.

Cheng, Z.B., Zhang, Y.N., Li, L.H. and Lv, H.Y. (2018), "Theoretical solution and analysis of the elastic modulus and foundation coefficient of coal-rock combination material", *Int. J. Mater. Sci. Res.*, **1**(1), 23-31.

Guo, J., Feng, G., Wang, P., Qi, T., Zhang, X. and Yan, Y. (2018), "Roof strata behaviour and support resistance determination for ultra-thick longwall top coal caving panel: A case study of the Tashan coal mine", *Energies*, **11**(5), 1041. https://doi.org/10.3390/en11051041.

Hock, E. and Brown, E.T. (1997), "Practical estimates of rock mass strength", *Int. J. Rock Mech. Min. Sci.*, **34**(8), 1165-1186. https://doi.org/10.1016/S1365-1609(97)80069-X.

Jirankova, E. (2012), "Utilisation of surface subsidence measurements in assessing failures of rigid strata overlying extracted coal seams", *Int. J. Rock Mech. Min. Sci.*, **53**, 111-119. https://doi.org/10.1016/j.ijrmms.2012.05.007.

Kirzhner, F. and Rozenbaum, M. (2001), "Behavior of the working fluid in mechanized support in permafrost", *J. Cold Reg. Eng.*, **15**(3), 170-185. https://doi.org/10.1061/(ASCE)0887-381X(2001)15:3(170).

Kong, D., Cheng, Z. and Zheng, S. (2019), "Study on failure mechanism and stability control measures in large-cutting-height coal mining face with deep-buried seam", *Bull. Eng. Geol. Environ.*, 1-15. https://doi.org/10.1007/s10064-019-01523-0.

Lei, C., Yang, J.H., Song, G.F. and Zhang, K. (2016), "Calculation of weighting interval and real-time working resistance based on beam elastic foundation method", *Electron. J. Geotech. Eng.*, **21**(5), 1931-1942.

Liu, F., Guo, Z., Lv, H. and Cheng, Z. (2018), "Test and analysis of blast wave in mortar test block", *Int. J. Rock Mech. Min. Sci.*, **108**, 80-85. https://doi.org/10.1016/j.ijrmms.2018.06.003.

Liu, X.J. and Cheng, Z.B. (2019), "Changes in subsidence-field surface movement in shallow-seam coal mining", *J. S. Afr. Inst. Min. Metall.*, **119**, 201-206. https://doi.org/10.17159/2411-9717/2019/v119n2a12.

Lv, H., Tang, Y., Zhang, L., Cheng, Z. and Zhang, Y. (2019), "Analysis for mechanical characteristics and failure models of coal specimens with non-penetrating single crack", *Geomech. Eng.*, **17**(4), 355-365. https://doi.org/10.12989/gae.2019.17.4.355.

Marschalko, M., Bednarik, M., Yilmaz, I., Bouchal, T. and Kubecka, K. (2011), "Evaluation of subsidence due to underground coal mining: an example from the Czech Republic", *Bull. Eng. Geol. Environ.*, **71**, 105-111. https://doi.org/10.1007/s10064-011-0401-8.

Masri, M., Sibai, M., Shao, J.F. and Mainguy M. (2014), "Experimental investigation of the effect of temperature on the mechanical behavior of Tournemire shale", *Int. J. Rock Mech. Min. Sci.*, **70**(9), 185-191. https://doi.org/10.1016/j.ijrmms.2014.05.007.

Sasaoka, T., Takamoto, H., Shimada, H., Oya, J., Hamanaka, A. and Matsui, K. (2015), "Surface subsidence due to underground mining operation under weak geological condition in Indonesia", *J. Rock Mech. Geotech. Eng.*, **7**(3), 337-344. https://doi.org/10.1016/j.jrmge.2015.01.007.

Suchowerska, A.M., Carter, J.P. and Hambleton, J.P. (2015), "Geomechanics of subsidence above single and multi-seam coal mining", *J. Rock Mech. Geotech. Eng.*, **8**(3), 304-313. https://doi.org/10.1016/j.jrmge.2015.11.007.

Vakili, A., and Hebblewhite, B.K. (2010), "A new cavability assessment criterion for longwall top coal caving", *Int. J. Rock Mech. Min. Sci.*, **47**(8), 1317-1329. https://doi.org/10.1016/j.ijrmms.2010.08.010.

Wang, J., Yang, S., Li, Y. and Wang, Z. (2015), "A dynamic method to determine the supports capacity in longwall coal mining", *Int. J. Min. Reclam. Environ.*, **29**(4), 277-288. https://doi.org/10.1080/17480930.2014.891694.

Wang, J., Yang, S., Li, Y., Wei, L., and Liu, H. (2014), "Caving mechanisms of loose top-coal in longwall top-coal caving mining method", *Int. J. Rock Mech. Min. Sci.*, **71**, 160-170. https://doi.org/10.1016/j.ijrmms.2014.04.024.

Xie, G.X., Chang, J.C. and Yang, K. (2009), "Investigations into stress shell characteristics of surrounding rock in fully mechanized top-coal caving face", *Int. J. Rock Mech. Min. Sci.*, **46**(1), 172-181. https://doi.org/10.1016/j.ijrmms.2008.09.006.

Xie, Y.S. and Zhao, Y.S. (2009), "Numerical simulation of the top coal caving process using the discrete element method", *Int. J. Rock Mech. Min. Sci.*, **46**(6), 983-991. https://doi.org/10.1016/j.ijrmms.2009.03.005.

Yang, T., Liu, J., Finklea, H., Lee, S., Epting, W.K., Mahbub, R., Hsu, T., Salvador, P.A., Abernathy, H.W. and Hackett, G.A. (2018), "An efficient approach for prediction of Warburg-type resistance under working currents", *Int. J. Hydrogen Energy*, **43**(32), 15445-15456. https://doi.org/10.1016/j.ijhydene.2018.06.076.

Yasitli, N.E. and Unver, B. (2005), "3D numerical modeling of longwall mining with top-coal caving", *Int. J. Rock Mech. Min. Sci.*, **42**(2), 219-235. https://doi.org/10.1016/j.ijrmms.2004.08.007.

Zhang, Y., Cheng, Z. and Lv, H. (2019). "Study on failure and subsidence law of frozen soil layer in coal mine influenced by physical conditions", *Geomech. Eng.*, **18**(1), 97-109. https://doi.org/10.12989/gae.2019.18.1.97.

CC

Notations

σ	bearing pressure each unit area
y	the subsidence of foundation
k_0	foundation coefficient
H	the thickness of cushion
k'	pull-pressing rigidity
E_1	the elastic modulus of coal mass
E_2	the elastic modulus of rock mass
r	coal to rock height ratio
b	the width of beam
k	the product of foundation coefficient
EI	the flexural rigidity of beam section
β	characteristic coefficient
y_0	initial settlement
θ_0	rotation angle
M_0	bending moment
Q_0	shear force
q_1	distributed load of key stratum
E_1I_1	the flexural rigidity of key stratum section
M_β	the maximum bending moment
E	elastic modulus
K	bulk modulus
G	shear modulus
TCCMF	top-coal caving mining face
OSL	overlying strata load
TCT	top-coal thickness
IRT	immediate roof thickness
TCEM	top-coal elastic modulus
IREM	immediate roof elastic modulus
FCD	first caving distance
TSL	total support load